Available online at www.sciencedirect.com

ScienceDirect

Ceramics International 39 (2013) 9511–9524

CERAMICS INTERNATIONAL

www.elsevier.com/locate/ceramint

Structural, electrical and optical properties of $Ba(Ti_{1-x}Yb_{4x/3})O_3$ ceramics

M. Ganguly[a], S.K. Rout[a,*], C.W. Ahn[b], I.W. Kim[b], Manoranjan Kar[c]

[a]Department of Applied Physics, Birla Institute of Technology, Mesra, Ranchi 835215, India
[b]Department of Physics and Energy Harvest-Storage Research Center, University of Ulsan, Ulsan 680-749, Republic of Korea
[c]Department of Physics, Indian Institute of Technology, Patna, Bihar, India

Received 26 April 2013; received in revised form 16 May 2013; accepted 16 May 2013
Available online 22 May 2013

Abstract

Ytterbium (Yb) doped barium titanates, $Ba(Ti_{1-x}Yb_{4x/3})O_3$ ($0.00 \leq x \leq 0.10$, in a step of 0.02) have been prepared through the solid state reaction route. Structural studies suggested a transition from tetragonal to cubic symmetry with increase in Yb^{3+} ion content, supported by Rietveld refinement technique. Photoluminescence study confirmed formation of shallow defects. The prepared materials are found to belong to violet, blue and green zone. Optical band gap values calculated from UV–visual diffuse reflectance spectra showed a decreasing trend with increase in Yb^{3+} ion concentration. Disk shaped pellets were prepared using PVA as binder. The effect of the partial presence of Yb^{3+} ions at Ti^{4+} ionic sites on the microstructure, dielectric and relaxor behavior of the ceramics were investigated. A drastic decrease in grain size is observed in the composition exhibiting the phase transition. Dielectric studies were performed over a wide temperature range from 15 K to 600 K at different frequencies. Normal ferroelectric character was obtained uptill $x \leq 0.04$ with subsequent increase in dielectric constant and a gradual decrease in the Curie temperature. Diffuse phase transition (DPT) was obtained at $x = 0.06$ while relaxor like behavior was observed for $x \geq 0.08$. A sharp decrease in Curie temperature as well as dielectric constant followed. The dielectric relaxation for $x = 0.08$ and 0.10 was modeled using the Vogel–Fulcher relation and a decrease in activation energy and an increase in frequency dispersion with increasing Yb^{3+} ion content was observed. *P–E* hysteresis loops showed a domain pinning effect which increased with increase in Yb^{3+} ion content resulting in a decrease in the values of remnant polarization.

Keywords: A. Solid state reaction; B. X-ray methods; C. Dielectric properties; C. Optical properties

1. Introduction

Perovskites-type oxides like $BaTiO_3$ (BT) is one of the extensively studied material in the past 50 years mainly as a dielectric material in MLCC [1,2]. It has also got wide application in electromechanical systems, electrooptical systems, pyroelectric detectors, piezoelectric actuators, MEMS, FeRAM [2–8]. Basically it acts as a good host matrix and various properties like the electrical resistance, dielectric constant, transition temperatures etc can be effectively controlled by doping with proper impurity ions, most commonly rare earth [9–12]. But the recent use of BT as a dielectric material in Ni based MLCC encounters a problem of oxygen vacancies (V_o) which is generated in BT layers during co-firing of BT and Ni metal in reducing atmosphere. Presence of these V_o spoils the insulating reliability of MLCC as these migrate to the vicinity of electrodes under DC electric field resulting in short circuit [13]. Doping of rare earth elements in BT lattice has been found to be effective in coping with such problems through V_o trapping by dopants [14–16]. A detailed mechanism of such interactions between V_o and rare earth dopants in BT lattice, both at A-site and B-site has been given by Honda et al. [17]. Thus with various rare earth doping in BT a lot of improvements in its properties have been made to meet various demands especially as a ceramic capacitor in MLCC [18–24].

Ytterbium (Yb) doped BT has been studied earlier [25–28,14]. Murillo et al. [28] have co-doped Er and Yb and have investigated the structural and morphological characteristics

*Corresponding author. Tel.: +91 9471555277.
E-mail addresses: skrout@bitmesra.ac.in, drskrout@gmail.com (S.K. Rout).

0272-8842/$ - see front matter © 2013 Elsevier Ltd and Techna Group S.r.l. All rights reserved.
http://dx.doi.org/10.1016/j.ceramint.2013.05.070

while Li et al. [27] have laid stress on the dielectric and tunability of Yb and other rare earth doped BT. Dunbar et al. [14] have made EPR investigation on various lanthanide including Yb doped BT. Of the recent studies Yao et al. [26] have presented a remarkable effect on the microstructural and dielectric properties of BT by codoping with Bi and Yb.

Though the reported research works done so far are remarkable but most of the studies include co-doping of Yb^{3+} ion with some other impurity ion. Singly doped Yb in BT has been mostly studied for optical purposes. A detailed survey of the various studies like structural, morphological, dielectric and optical study simultaneously is rarely available in Yb doped BT based ceramics. This article is based on such type of investigation in Yb doped BT ceramics, through charge compensation mechanism with a core aim to improve the insulating reliability of MLCC.

BT has a perovskite structure (ABO_3) where Ba occupies the A-site and Ti the B-site. Rare earths are incorporated at both the sites. Choice is generally made by comparing the radii of the rare earth to be doped and the site to be incorporated. Here Yb^{3+} ion is incorporated at the B-site as its radius is much more comparable to Ti^{4+} ion rather than Ba^{2+} ion. It is expected to behave as an acceptor according to the equation

$$Ti^{4+} \rightarrow Yb^{3+} + h \text{ (where “h” denotes a hole)}$$

Yb doped BT ceramics have been prepared according to the equation

$$BaCO_3 + (1-x)TiO_2 + (2x/3)Yb_2O_3 \rightarrow BaTi_{1-x}Yb_{4x/3}O_3 + CO_2(\uparrow)$$

(where $x = 0.00$, 0.02, 0.04, 0.06, 0.08 and 0.10).

Excluding the composition $x = 0.00$, all the other compositions are non-stoichiometric, exhibiting excess of Yb^{3+} ion in the prepared perovskite type solid solutions according to the structural formula

$BaTi_{1-x}Yb_x\bullet_{x/3}TiO_3$, where $\bullet$ denotes excess amount of Yb doped in the perovskite structure.

The above mechanism of doping has been chosen following a charge compensation method, as the valency of the B-site is (+4) while that of Yb is (+3). The excess amount of Yb^{3+} ion content in the ceramics forms a secondary phase as shown below

$$TiO_2 + Yb_2O_3 \rightarrow Yb_2Ti_2O_7 \quad (3)$$

Investigations on these prepared ceramics were carried out taking into account the above fact [25,26,29].

2. Experimental

2.1. Synthesis of $BaTi_{1-x}Yb_{4x/3}O_3$ by solid state reaction route

$BaTi_{1-x}Yb_{4x/3}O_3$ (x=0.00, 0.02, 0.04, 0.06, 0.08 and 0.10) ceramics were prepared through solid state reaction route from reagents $BaCO_3$ (99% Pure, Merck, India Ltd.), TiO_2 (99% Pure, Merck, India Ltd.) and Yb_2O_3 (99.99% Pure, Sigma-Aldrich, USA). Powders were mixed in an appropriate amount and grinded with distilled water in an agate mortar. The homogeneous powder was milled in a FRITSCH “Pulverisette 5” planetary mill for 10 h with Zirconium balls (5 mm diameter) and then heated at 1200 °C for 12 h. Regular grinding and heating was followed by final calcination at 1400 °C for 4 h.

2.2. Characterizations

Structural characterization was done by XRD using CuKα radiation from 15° to 80° with a step size of 0.02° and scanning rate of 1 deg/min. The Fourier Transform Infra red (FTIR) spectra was recorded at room temperature by the standard KBr pellet technique in a Perkin-Elmer Fourier

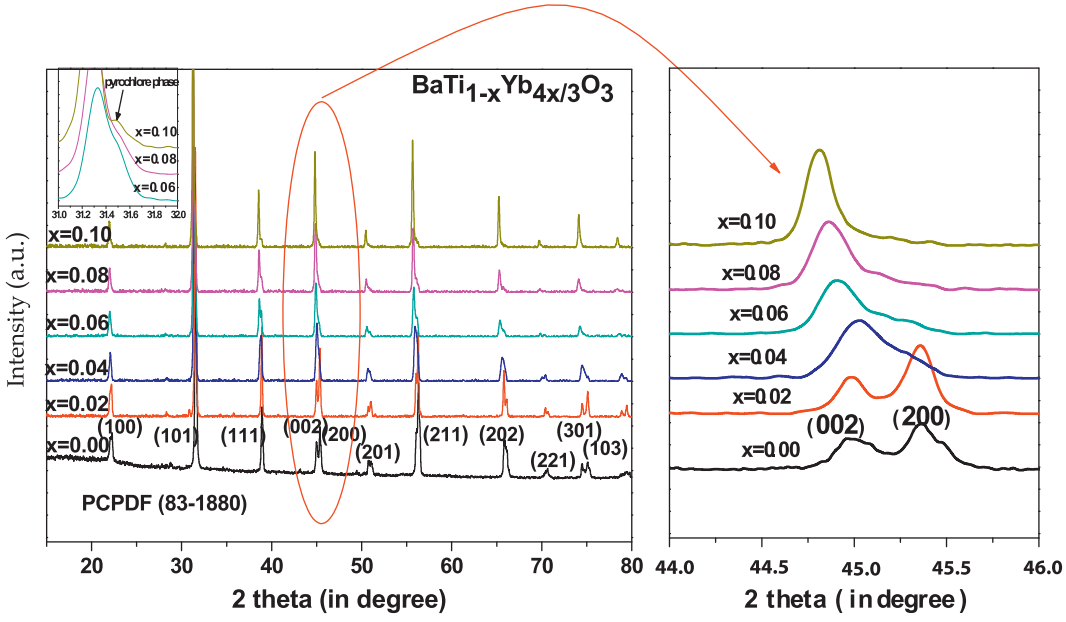

Fig. 1. Room temperature XRD patterns of $BaTi_{1-x}Yb_{4x/3}O_3$ powders along with shifting and merging of peak of $BaTi_{1-x}Yb_{4x/3}O_3$ with increase in doping concentration.

Transform Infra Red Spectrophotometer (Spectrum 1000), Japan. Raman spectroscopic studies followed thereafter (Seki Technotron with excitation 514 nm). Photoluminescence study was done using a Hitachi Fluorescence Spectrophotometer (model-F2500) to study the luminescence efficiency of the doped ceramics. UV–visual study was done to calculate the band gap using a Cary 5G (Varian, USA) spectrophotometer.

Calcined powders were pressed uniaxially under pressure 60 kg/cm^2 in a hydraulic press to form disk shaped pellets of 10 mm diameter and 2 mm thickness with 5% polyvinyl alcohol as the binder. Sintering of the pellets was done at 1400 °C for 10 h for x=0.00 while at 1480 °C for 10 h for x=0.02–0.10, to obtain optimal shrinkage and compactness. Bulk densities calculated according to Archimedes Principle were found to be greater than 95% of their respective theoretical values. Microstructural study was done using a Scanning Electron Microscope (JSM-6390LV). Dielectric study of the sintered and densified pellets was done over a wide temperature range from 15 K to 573 K by the HP4294A system. A Sawyer–Tower circuit at room temperature measured the ferroelectric P–E hysteresis loops.

3. Results and discussion

Fig. 1 shows the XRD pattern of $Ba_{1-x}Yb_{4x/3}TiO_3$ ceramic powders calcined at 1400 °C for 4 h. The compositions with lesser Yb^{3+} ion concentration show the reflections of single phase perovskite structure. However a secondary phase reported as pyrochlore phase ($Yb_2Ti_2O_7$) is identified at higher Yb doped ceramics most prominently in x=0.10 as shown in inset [26]. The excess amount of Yb_2O_3 (beyond the solubility limit) reacts with TiO_2 to form this phase and as its amount increases it can be identified clearly [25,29]. The diffraction pattern of all ceramics within the 2θ range of 44°–46° is shown in a magnified scale for clarity. The presence of (002) (200) peaks in x=0.00–0.04 suggests a tetragonal symmetry while in

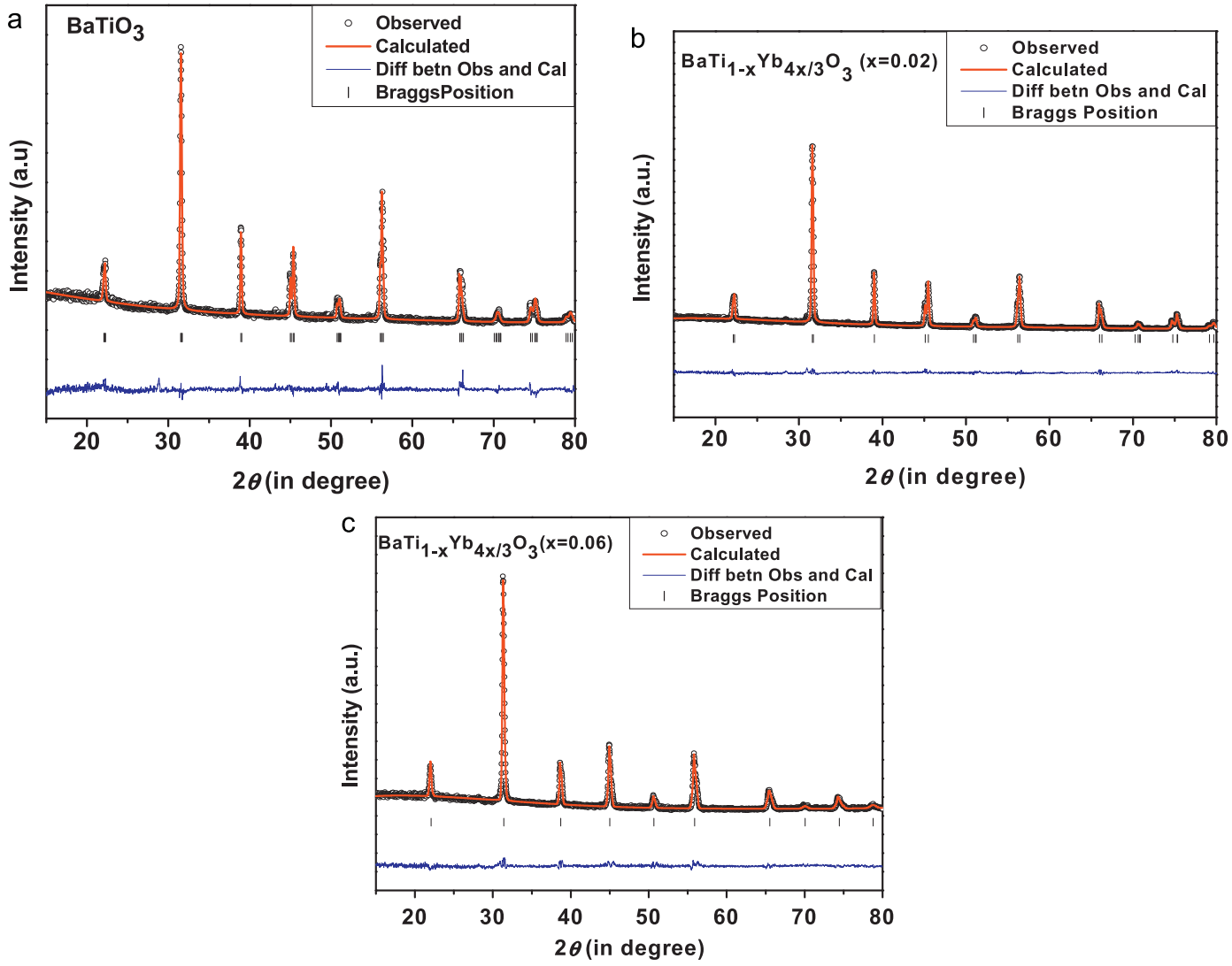

Fig. 2. Observed (°), calculated (–) and residual X-ray powder diffraction pattern of $BaTi_{1-x}Yb_{4x/3}O_3$ compositions (a) x=0.00 (b) x=0.02 and (c) x=0.06 revealed from Rietveld's powder structure refinement analysis. Peak positions of the phases are shown at the base line as small marker. Positional parameters for the composition x=0.00, 0.02 (P4mm) are: Ba at 1a(0,0,0), Ti/Yb at 1b(0.5,0.5,0.524), O_1 at 1b(0.5,0.5,-0.005), and O_2 at 2c(0.5,0,0.427) and for the composition x=0.06 (Pm-3m) are: Ba at1a(0,0,0) Ti/Yb at 1b (0.5,0.5,0.5) and O at 3c(0,0.5,0.5).

$x \geq 0.06$ merging of both the peaks gives a better indexing by cubic symmetry at room temperature. Shifting of peak towards lower angle indicates an increase in the lattice parameters with increase in Yb concentration. The radius of Ti^{4+} ion is 0.6 Å while that of Yb^{3+} ion is 0.86 Å for a state with co-ordination number 6. Hence it is obvious that substitution of higher radii Yb ion at the lower radii Ti ionic site results in increase in cell parameters and hence in cell size. A decrease in tetragonality of the ceramics with increase in Yb^{3+} ion content takes place leading to cubic symmetry.

Structural refinement was carried out for the compositions x=0.00, 0.02 and 0.06 using Rietveld's refinement program "Full Prof" and the final output is shown in Fig. 2(a)–(c). From structural refinement it is confirmed that $x=0.00$ and 0.02 has tetragonal symmetry with space group P4mm while $x=0.06$ has cubic symmetry at room temperature. The initial parameters are taken from the standard Wycoff position table. The refinement produced satisfactory agreement factors and lattice parameters which are listed in Table 1.

FTIR technique was employed to study the influence of additives in the ceramics. As the ferroelectricity in perovskite ferroelectric materials depends greatly on the vibration of the crystal lattice so FTIR is an effective technique to study the correlation between physical properties and microstructure of such materials. The FTIR spectra of all the ceramics at room temperature are given in Fig. 3 while the inset shows shift of the Ti–O_I absorption peak. A strong absorption peak for pure BT ($x=0.00$) is obtained at 524.64 cm^{-1}. This corresponds to the stretching normal vibration of Ti–O_I octahedron [30–32]. This mode is very important because the direction of stretching normal vibration is along with that of spontaneous polarization in BT with tetragonal symmetry [30]. Absorption peaks for the same mode in $x=0.02$, 0.04, 0.06, 0.08 and 0.10 are obtained at 527.94, 530.61, 536.37, 552.25 and 563.06 cm^{-1} respectively. Thus a shift towards higher energy is observed. As observed from XRD a decrease in tetragonality, followed by a change in symmetry from tetragonal to cubic is noticed with subsequent Yb substitution. This should shorten the distance between Ti^{4+} and O^{2-} enhancing the bond strength. As explained by Jin et al. [33] according to equation

$$\frac{\nu^{BT}_{Ti-O}}{\nu^{BTY}_{M-O}} = \sqrt{\frac{\mu_{M-o}}{\mu_{Ti-o}}}\sqrt{\frac{f^{BT}_{Ti-O}}{f^{BTY}_{M-O}}} \quad (4)$$

Table 1
Results of Rietveld refinement of X- ray diffraction data of $Ba_{1-x}Yb_{4x/3}TiO_3$ measured at room temperature for the tetragonal region with space group P4mm for $x=0.00$, 0.02 while for the cubic region with space group Pm-3m for $x=0.06$.

Parameters	$x=0.00$	$x=0.02$	$x=0.06$
Lattice parameter ($a=b$) (Å)	3.9957	3.9992	4.0260
Lattice parameter (c) (Å)	4.0256	4.0293	4.0260
Volume (Å^3)	64.270	64.443	65.258
R_p	7.95	6.46	7.40
R_{wp}	10.60	8.56	9.54
R_{exp}	7.71	6.87	7.20
Goodness of fit (χ^2)	1.90	1.55	1.75

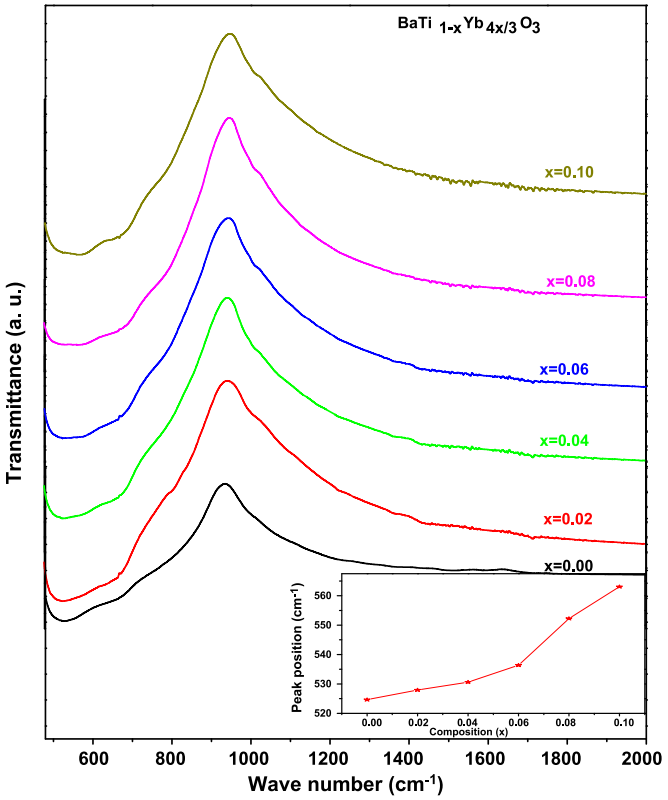

Fig. 3. FTIR spectra of $BaTi_{1-x}Yb_{4x/3}O_3$ at room temperature.

where $BT=BaTiO_3$, $BTY=BaTi_{1-x}Yb_{4x/3}O_3$, M is the B-site metal ion (Ti/Yb), μ is the reduced mass and f is the force constant. Since the BTY ceramics have two B-site cations, so Eq. (4) can be expressed as

$$\frac{\nu^{BT}_{Ti-O}}{\nu^{BTY}_{M-O}} = \sqrt{k}\sqrt{\frac{f^{BT}_{Ti-O}}{f^{BTY}_{M-O}}} \quad (5)$$

where

$$k = \frac{(1-x)\mu_{Ti-O} + (4x/3\mu_{Yb-O})}{\mu_{Ti-O}} \quad (6)$$

As $k>1$, so a shift of absorption band towards high wave number indicates $f^{BTY}_{M-O} > f^{BT}_{Ti-O}$. Hence the M–O bond becomes stronger with subsequent Yb doping than that of undoped BT.

A theoretical explanation can be given through the tolerance factor (t) which is unity for an ideal perovskites (cubic). The value of this factor can be calculated through the following equation [32]:

$$t = \frac{R_O + R_A}{\sqrt{2}(R_O + R_B)} \quad (7)$$

For $BaTi_{1-x}Yb_{4x/3}O_3$ the tolerance factor is given as

$$t = \frac{R_O + R_{Ba^{2+}}}{\sqrt{2}[(R_O + (1-x)R_{Ti^{4+}} + (4x/3)R_{Yb^{3+}})]} \quad (8)$$

Taking R_O=1.4 Å, R^{2+}_{Ba}=1.6 Å, R^{3+}_{Yb}=0.86 Å and R^{4+}_{Ti} =0.65 Å, the values of tolerance factors obtained from Eq. (7) along with their respective absorption peak positions are listed in Table 2. Successive decrease in the values of

Table 2
Tolerance factor and shift in absorption peak of $Ba_{1-x}Yb_{4x/3}TiO_3$ ceramics.

Composition	Absorption peak (cm^{-1})	Tolerance factor (t)
$x=0.00$	524.64	1.060
$x=0.02$	527.94	1.030
$x=0.04$	530.61	1.025
$x=0.06$	536.37	1.020
$x=0.08$	552.25	1.015
$x=0.10$	563.06	1.010

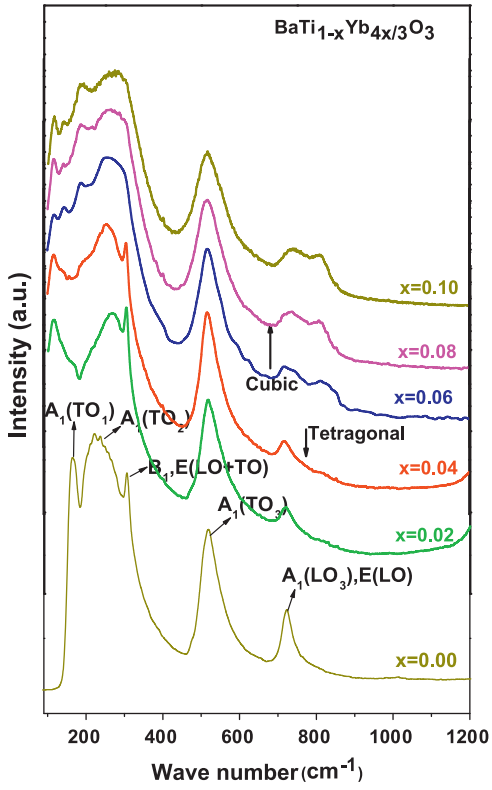

Fig. 4. Raman spectra of $BaTi_{1-x}Yb_{4x/3}O_3$ at room temperature.

tolerance factor is noticed with Yb doping and increases in its concentration with an approach towards unity (cubic symmetry). Hence it is quite obvious that bond strength increases.

Optical modes of cubic BT transform according to the $3F_{1u}+1F_{2u}$ irreducible representation. The detailed mechanism behind the origin of Raman spectra in tetragonal BT and doped cubic BT has been given in our earlier works [34]. Fig. 4 shows the Raman spectra for the series of samples. Mode assignment shows appearance of $A_1(LO_3)$ mode at 721 cm^{-1}, a feature of tetragonal BT, which arises for phonons propagating along the c axis. The E(LO) mode also arises simultaneously for phonons propagating in ab plane. In the tetragonal phase the separation between the A_1 and E component of F_{1u} mode is negligible. Presence of B_1 mode at 305 cm^{-1} along with overlapping of E(TO) and E(LO) is clearly observable in $0.00 \leq x \leq 0.04$. This overlapping may be due to random orientation of crystallites. This mode, arising from out-of-phase vibration of oxygen ions only, disappears from $x \geq 0.06$. This confirms the phase transition taking place, as observed from XRD study, from tetragonal symmetry (P4mm) to cubic symmetry (Pm-3m) [34–36,37].

The behavior of the soft mode frequency (A_1+E) in solid solutions is characterized by short range force constant, long range interactions, and masses of the ions involved. A decrease in intensity and broadening in the $A_1(LO_3)$, E(LO) mode is observed with subsequent increase in Yb content. This mode shows a second peak on the high frequency side (at 721 cm^{-1} and 810 cm^{-1}), clearly noticeable from $x \geq 0.06$. It has been reported that mode frequency of this mode changes in a series of complex perovskites as a function of perovskite unit cell and with changes in ionic radii. Though neither A or B ions move in this vibration, the mode still reflects changes in the perovskite structure. In this mode only the oxygen ions move. Doping BT with Yb results in presence of different radii ions at the B-site. This results in formation of inequivalent oxygen octahedral that changes the spacing between A and B ions. A change in their bonding also takes place. Again a decrease in the B–O–B bond and respective bond angle also takes place. This modifies the short range Ti–O force constant, disturbing the Ti-(3d) and O-(2p) hybridization. Since Raman spectroscopy is very sensitive to instantaneous atomic shifts from regular sites, so mode frequency changes, resulting in appearance of extra peaks. It has already been reported that distortion in the Ti–O–Ti bond not only changes the soft mode parameter but also results in appearance of extra band in the Ti–O vibration (≥500 cm^{-1}) [37–39]. Similar feature has been observed not only during a composition induced phase transition but also during pressure induced phase transition in BT [39,40]. Another feature is that spacing between these two peaks gradually decreases with further increase in Yb content and the two peaks are noticed to move towards each other. Hence it can be concluded that the anisotropy in the short range interatomic forces decreases with further increase in Yb content. Again with subsequent increase in Yb content, formation of secondary phase also takes place, which has been reported to generally segregate at the grain boundaries [26]. This generates some stress which increases with subsequent increase in the concentration of Yb. Disorder in polycrystalline BT materials is also due to other mechanism such as grain boundary and intergrain stresses [40]. Thus stress which can break Raman selection rules, may be the reason behind the observed shift of the peaks. Generally $A_1(LO_3)$ mode is observed to make blue shift under stress while $A_1(TO_3)$ mode in the range 500–600 cm^{-1} do not show any significant induced frequency shift [41].

Asymmetric, broad, intense modes at 518 cm^{-1} and centered at 219 cm^{-1} [A_1(TO)] are observed. A decrease in the intensity and broadening in the $A_1(TO_3)$ mode at 518 cm^{-1} is clearly noticeable in $x \geq 0.08$. This mode arises from the motion of the Ti and O_1 ions against O_2 and O_3 ions, which are located in the perpendicular plane. This is also associated with change in the Ti–O–Ti bond. The $A_1(TO_2)$ mode shifts towards higher energy values along with a broadening effect. Merging and splitting of the $A_1(TO_1)$ and $A_1(TO_2)$ modes are featured from $x \geq 0.06$. It has been reported that low energy F_{1u} mode (A_1 and E) are very sensitive to Ti–O bond as it correspond to motion

of Ti ion against oxygen octahedron [37]. Due to higher radii Yb substitution at the lower radii Ti-site, the Ti–O–Ti bond length changes along with bond angle that makes all the above features occur. Some anti-resonance effect (dip) is obtained at around 180 cm^{-1} which may be an interference effect due to anharmonic coupling between $A_1(TO_1$ and $TO_2)$ modes [35]. A sharp line at 160 cm^{-1} is obtained in $0.00 \leq x \leq 0.04$. This corresponds to vibration of Ba ions against TiO_6 octahedron. This mode is noticed to soften from $x \geq 0.06$. All these are suggestive to decrease in tetragonality with subsequent increase in Yb content leading to the phenomenon of phase transition.

Table 3
Variation in F.W.H.M. and peak position of A_1 mode of $BaTi_{1-x}Yb_{4x/3}O_3$ w.r.t x at room temperature.

Composition	Peak position of $A_1(TO_3)$ mode (cm^{-1})	F.W.H.M. of $A_1(TO_3)$ mode (cm^{-1})	Peak position of $A_1(LO_3)$, E (LO) mode (cm^{-1})	F.W.H.M. of $A_1(LO_3)$, E (LO) mode (cm^{-1})
$x=0.00$	518	55.27	721	23.65
$x=0.02$	516	46.20	716	28.06
$x=0.04$	516	50.73	719	28.65
$x=0.06$	516	50.90	717, 810	75.73, 51.39
$x=0.08$	516	64.87	738, 806	71.65, 25.77
$x=0.10$	516	61.83	741, 805	98.70, 30.48

The half width variation and peak positions for A_1 and E (LO) modes (after Gaussian fit) w.r.t. composition is given in (Table 3). For the $A_1(TO_3)$ mode no shifting of peaks but increase in width is observed with subsequent increase in Yb content. A similar increase in width for the peak at 721 cm^{-1} but decrease in width for the peak at 810 cm^{-1} (from $x \geq 0.06$) is observed, with subsequent increase in Yb content. Broadening in the modes may be due to introduction of disorder in the lattice of the doped samples. Yb incorporation causes local distortion and breaks partially the translation symmetry in BT. Thus Raman selection rules gets relaxed and accordingly broadening in modes takes place.

The microstructures of the polished and thermally etched sections of $BaTi_{1-x}Yb_{4x/3}O_3$ are shown in Fig. 5 (a) and (b). Disc/plate like morphology with large size grains (average size ≥ 50 μm) is obtained for undoped BT ($x=0.00$). These may be ferroelectric domains of BT which are clearly visible at higher resolution. Spiral concentric grain growth is also clearly visible. The doped ceramics are found to be dense with well defined grain boundary and with clearly visible grains of much smaller sizes than that of undoped BT. The average grain size of $x=0.02$ and 0.04 (tetragonal symmetry) are found to be

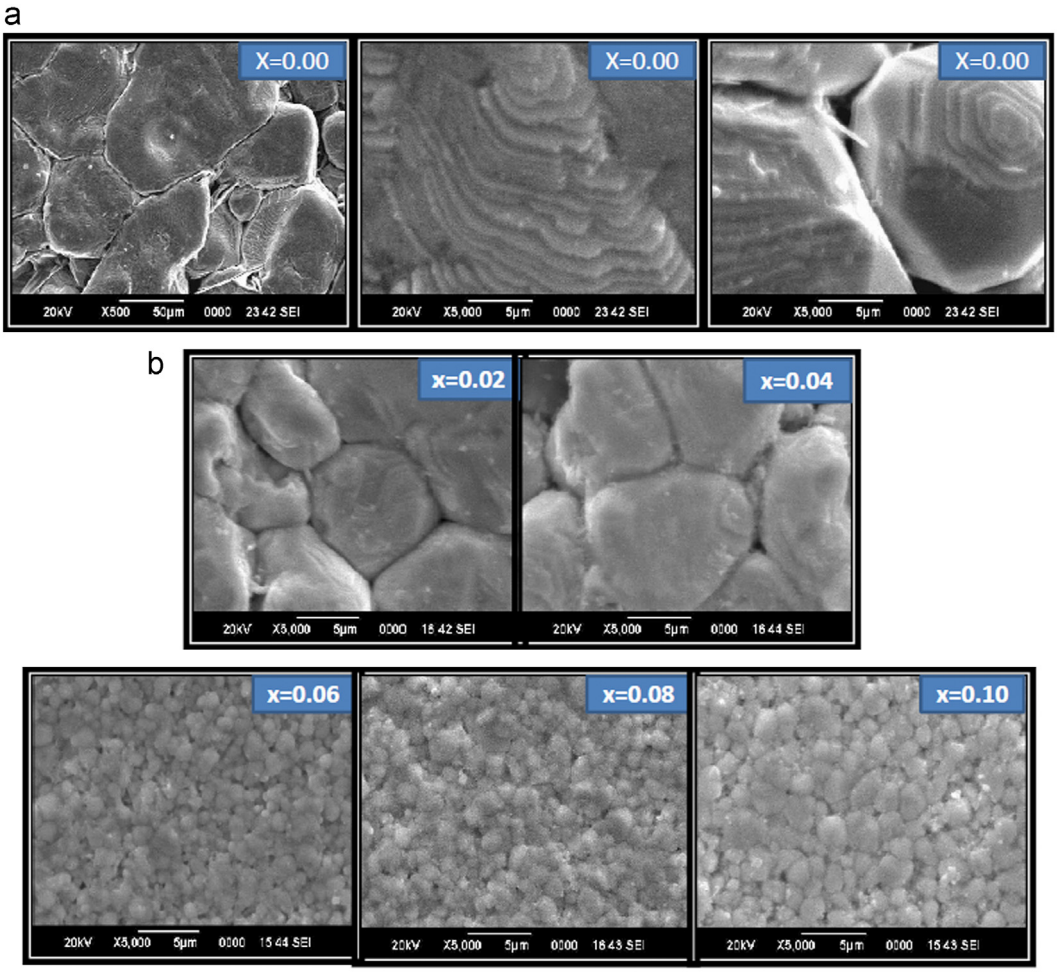

Fig. 5. SEM micrographs of $BaTi_{1-x}Yb_{4x/3}O_3$.

10 μm exhibiting similar irregular shaped, domain like features that disappears in $x \geq 0.06$ [25,42]. The grains in $0.06 \leq x \leq 0.10$ (cubic symmetry) are quite smaller (average size ≈1 μm) but uniform. BT doped with Yb in low concentrations has been reported to feature large grains similar to $x=0.02$ and 0.04 [25,26]. Variation in the kinetics of matter transport over long distances results in irregular shape of the grains at lower Yb^{3+} ion content.

Microstructural features are mainly governed by transport of matter during heating process. Solid state synthesis method starts with milling of raw materials, during which a reduction of average particle size occurs. Upon heat treatment, diffusion starts at the contact points of the particles which over sintering lead to formation of grains. Matter transport at long distances leads to the formation of larger grains. Here in the prepared ceramics with subsequent increase Yb concentration grain size decreases. Hence it can be concluded that the diffusion of Yb^{3+} ion in BT lattice decreases accordingly. Substitution of higher radii ion in B-site may be associated with decrease in grain size with increase in doping content, due to slow diffusion of the higher radii ion at the smaller radii site. Also the formation of the secondary phase $Yb_2Ti_2O_7$ may hinder the grain growth for the highly doped ones. Yb-doped specimen has shown some segregation of Yb rich secondary phase at the grain boundary which limits the solubility of Yb in BT [26,42].

Thus it can be considered that a large modification in the microstructure of BT occurs on doping with Yb inhibiting grain growth especially at 6% and above Yb content.

Dielectric behavior as a function of temperature at different frequencies is shown in Fig. 6 while the variation in dielectric loss at higher temperature is shown as insets. Dramatic decrease in T_{c-t} (cubic to tetragonal), while increase in T_{t-o} (tetragonal to orthorhombic) and T_{o-r} (orthorhombic to rhombohedral) transition temperatures are observed with subsequent increase in Yb concentration. In $x \geq 0.06$ the T_{c-t} transition shifts below room temperature. Hence it can be concluded that $0.00 \leq x \leq 0.04$ have a tetragonal symmetry while $0.06 \leq x \leq 0.10$ have cubic symmetry at room temperature. This is in consistent with the room temperature XRD, Rietveld refinement and Raman data of the ceramics. Decrease in the value of dielectric constant is observed with increase in frequency. Higher values of DC at lower frequency may be due to space charge polarization [43]. Pinching effect [44] is observed where T_{c-t}, T_{t-o} and T_{o-r} move towards each other with subsequent increase in Yb concentration. The T_{c-t} shifts towards lower value while T_{t-o} towards higher one and finally merge to give a broad transition. Such shifting of peaks is observed uptill $x \leq 0.04$ and from $x \geq 0.06$ merging of peaks results in broad transition. Frequency dependent dielectric behavior is observed only for $x=0.08$ and $x=0.10$. The value of T_m of these two ceramics shifts towards higher temperatures on increasing the frequency. Another feature is that there is a sharp decrease in the values of dielectric constants from $0.00 \leq x \leq 0.04$ (5699–6754 at 10^4 Hz) to $0.06 \leq x \leq 0.10$ (2333–1104 at 10^4 Hz). The ceramics exhibit very low dielectric loss.

Decrease in T_{c-t} with increase in rare earth content has been well reported in literature [42–45]. This basically is an indication of a decrease in tetragonality. Shrinkage of unit cell takes place off centering the Ti^{4+} ion out of the octahedral site. Thus the coupling between the TiO_6 octahedra weakens.

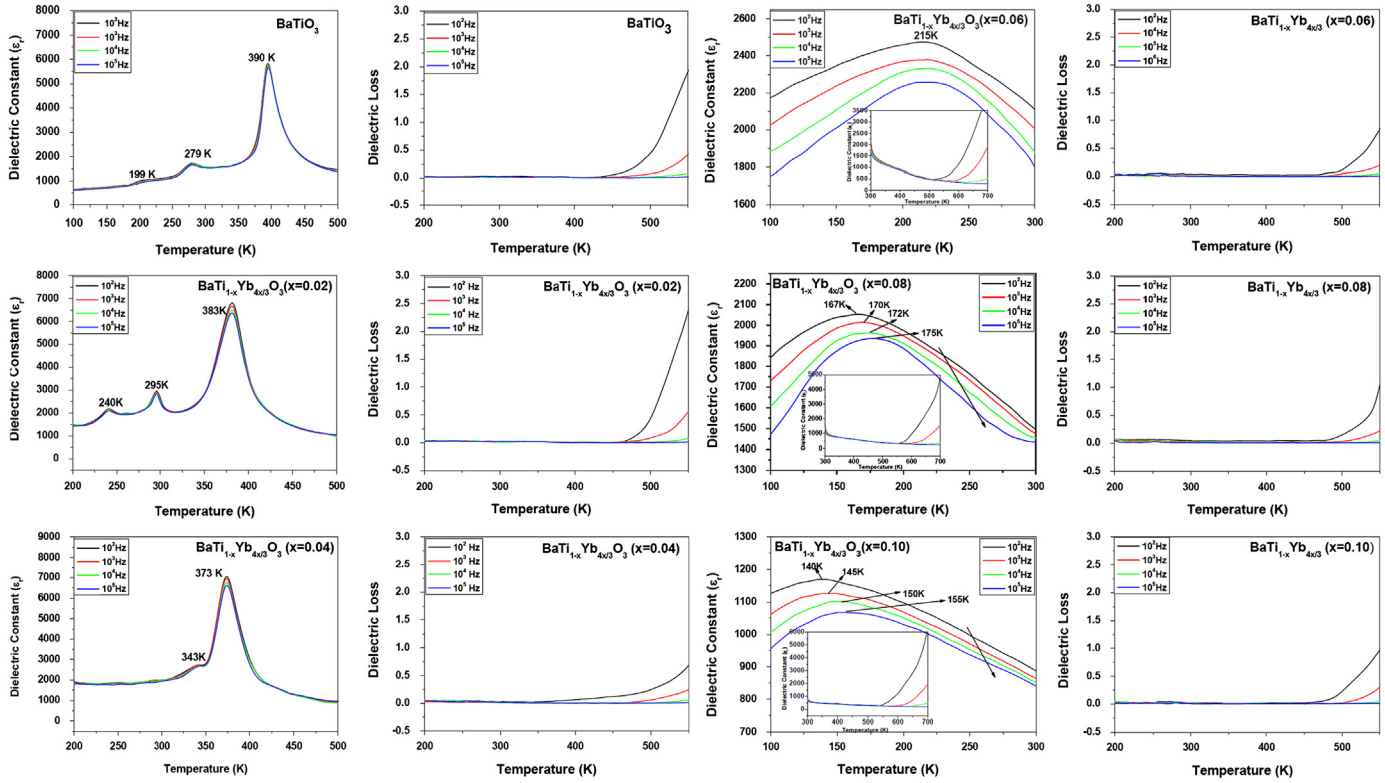

Fig. 6. Dielectric constant and dielectric loss as a function of temperature of $BaTi_{1-x}Yb_{4x/3}O_3$ at various frequencies.

This results in a strong decrease in T_{c-t} (T_c is directly related to the displacement of cation from the center of the octahedral site to its position in the polar phase) [43,45,46]. Now, it is a genuine fact that dielectric constant is directly related to tetragonality, grain size and density. So the fall in dielectric constant values in the ceramics with higher Yb content (cubic symmetry) can be attributed to the dramatic decrease in grain size and tetragonality. The slight increase in its value from x=0.00 to x=0.04 may be due to increase in the density of the ceramics. But on further increase in Yb content the dielectric behavior is mostly dominated by grain size and tetragonality rather than other factors.

Dielectric stiffness ($1/\varepsilon$) at 10 KHz from x=0.06–0.10 (Fig. 7) are found to deviate from Curie–Weiss law. The Curie–Weiss temperature (T_0) is found to be greater than T_m. This indicates a relaxor like behavior. The parameter ΔT_m[(T_{cw}–T_m), where T_{cw} denotes the deviation temperature of permittivity from C–W law, T_m is the dielectric maximum temperature] describes the degree of deviation from Curie–Weiss law. The modified C–W law for such ceramics is given as

$$\frac{1}{\varepsilon}-\frac{1}{\varepsilon_{max}}=\frac{(T-T_{max})^{Y}}{C} \tag{9}$$

where C and γ are constants; ε_{max} is the maximum dielectric constant at the transition temperature T_{max}. This law for x=0.06, 0.08 and 0.10 are plotted in Fig. 8. Linear relationships are observed. Slopes of the fitting curve give the values of relaxation strength or degree of diffuseness, γ. It is: (1) for normal ferroelectrics following C–W law and (2) for ideal relaxor ferroelectrics (a quadratic dependency describes diffuse phase transition) [43,47]. The obtained values of γ give a clear indication that the materials are disordered and transitions are of diffused type.

In perovskites, relaxor like behavior is generally attributed when at least two different cations occupy the same crystallographic site. When higher radii Yb^{3+} ion replace Ti^{4+} ion, a modification occurs followed by a change in the symmetry with increase in Yb content. The Ti^{4+} ion occupying the octahedral site becomes off centered giving rise to differently polarized microregions existing in macroregions, diluting the ferroelectric character. With subsequent increase in Yb content this displacement in the tetragonal positions is more and more affected. Such positional disorders induces compositional inhomogeneity resulting in diffused phase transition and relaxor like behavior and at higher Yb concentration this behavior is prominent and not at lower concentration. Also, as already explained, the formation of the secondary phase at higher Yb content develops stress in the grains which adds to the cause of relaxor character. Indication for such type of behavior is also evident from frequency shift and increase in half width of $A_1(LO_3)$, E(LO) mode of Raman spectra. It is worth mentioning that this structural disorder and formation of microdomains with local polarization induced due to doping results in different local Curie points. [48,49].

The plots of $\log(\upsilon)$ versus $(1/T_m)$ are shown in Fig. 9 for x=0.08 and 0.10. The nonlinear nature indicates that the data

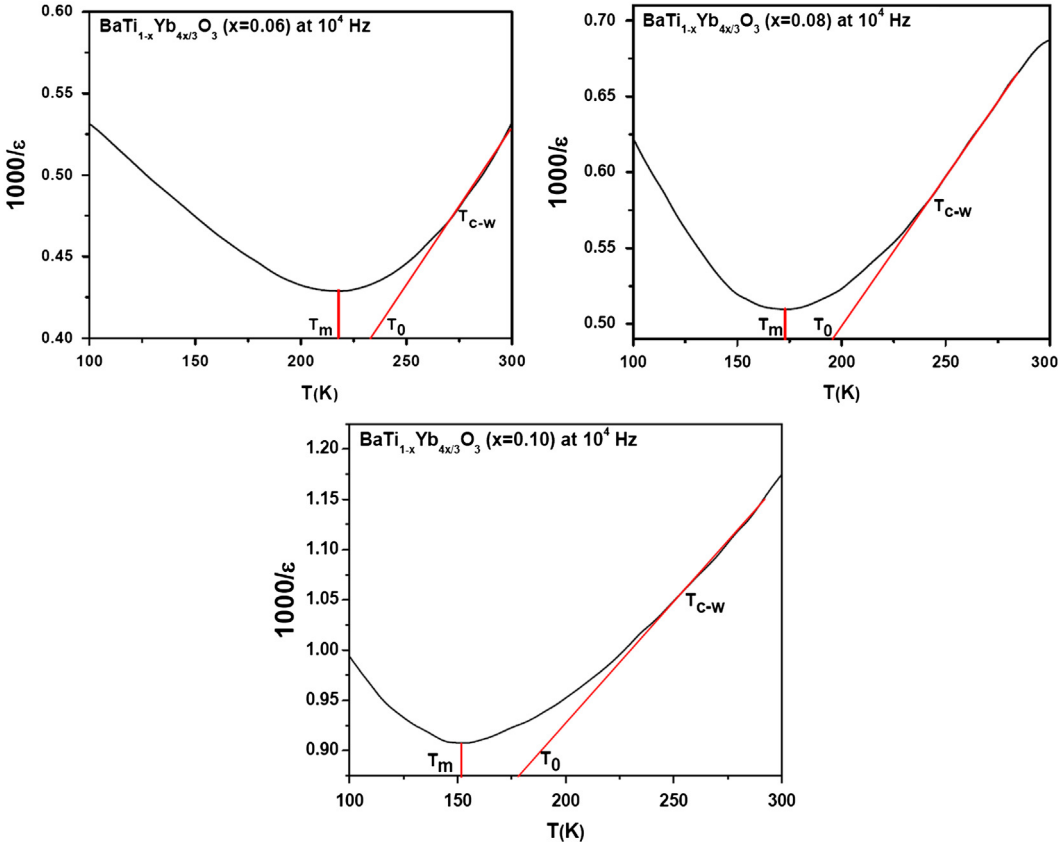

Fig. 7. Dielectric stiffness as a function of temperature for x=0.06, 0.08 and 0.10 at 10 kHz.

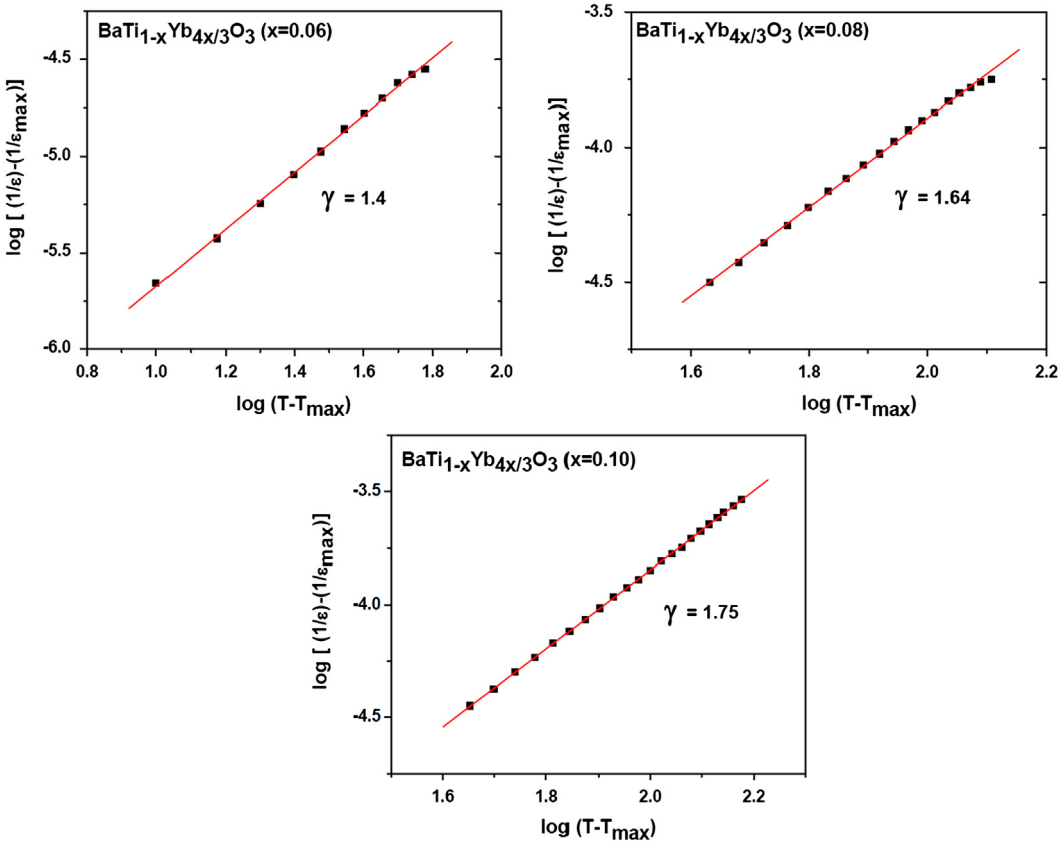

Fig. 8. Plot of $\log(T-T_{max})$ vs. $\log[1/\varepsilon-1/\varepsilon_{max}]$ for $x=0.06$, 0.08 and 0.10 at 10 kHz.

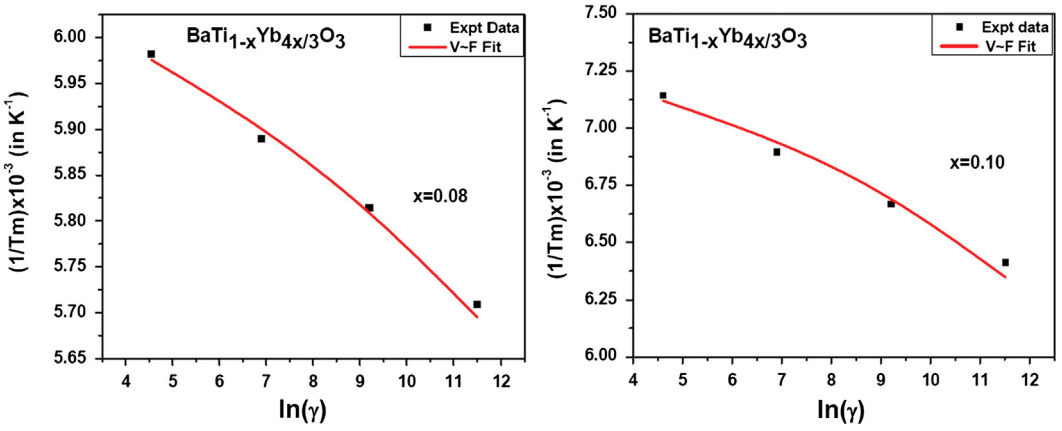

Fig. 9. $1/T_m$ as a function of measured frequency of $BaTi_{1-x}Yb_{4x/3}O_3$ for $x=0.08$ and 0.10. The symbols are the experimental data points and the line is corresponding fitting to the Vogel–Fulcher relationship.

cannot be fitted with a simple Debye equation. To analyze the relaxation features of the ceramics the experimental curve for these compositions were fitted using the Vogel–Fulcher formula [47]

$$\upsilon = \upsilon_0 \exp\left[\frac{-E_a}{k_B(T_m - T_f)}\right] \quad (10)$$

where υ_0 is the attempt frequency, E_a is the activation energy, k_B is the Boltzman constant and T_f is the freezing temperature. T_f is regarded as the temperature where the dynamic reorientation of the dipolar cluster polarization can no longer be thermally activated. The fitting curves for these ceramics are shown (Fig. 9). The fitting parameters are $E_a=0.049$ eV, $T_f=145$ K and $\upsilon_0=1.74\times10^{13}$ Hz for $x=0.08$ while for $x=0.10$ the values are $E_a=0.021$ eV, $T_f=123$ K and $\upsilon_0=1.18\times10^{8}$ Hz. The close agreement of the data with the V–F relationship suggests a relaxor like behavior. The various parameters obtained from temperature dependent dielectric study for $x=0.06$, 0.08 and 0.10 at 10 kHz are listed in Table 4. For $x=0.06$, since no frequency dependent character

Table 4
Parameters obtained from temperature dependent dielectric study of $BaTi_{1-x}Yb_{4x/3}O_3$ ($x=0.06$, 0.08 and 0.10) at 10^4 Hz.

Parameters	$x=0.06$	$x=0.08$	$x=0.10$
T_m (K)	215	172	150
T_o (K)	233	195	178
T_{cw} (K)	270	241	239
ΔT_m ($T_{cw}-T_m$) (K)	55	69	89
ε_{max}	2333	1965	1104
γ	1.4	1.64	1.75

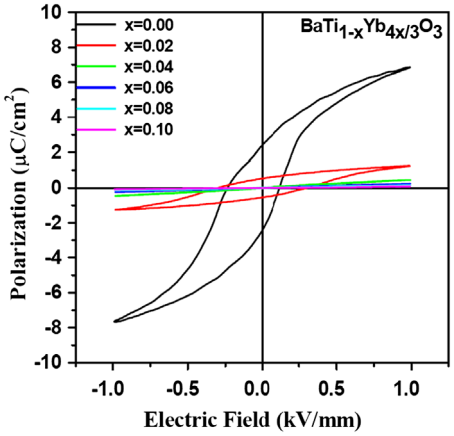

Fig. 10. *P–E* hysteresis loop of $BaTi_{1-x}Yb_{4x/3}O_3$ ($0.0\leq x\leq 0.10$).

of T_m is obtained so a fit to Vogel–Fulcher law was not performed. Thus though an indication of relaxor like behavior is obtained in this ceramic yet it cannot be characterized as a typical relaxor.

The *P–E* hysteresis loops of pure and doped ceramics at room temperature are shown in Fig. 10. These hysteresis loops were measured using a maximum applied electric field of 1 kV/mm at a frequency of 50 Hz. It is noticed that the hysteresis loops approach saturation under such an electric field. The values of the remnant polarizations obtained are 2.42 μC/cm^2, 0.54 μC/cm^2, 0.04 μC/cm^2 and coercive fields are −0.23 kV/mm, −0.30 kV/mm and −0.24 kV/mm respectively from $x=0.00$ to $x=0.04$ while for $x=0.06$ to $x=0.10$ both the values dropped to almost zero giving a linear *P–E* behavior. Clearly a steady decrease in the ferroelectric behavior of the samples is obtained with subsequent increase in Yb content. For $0.06\leq x\leq 0.10$, a linear *P–E* behavior suggests the structure to be normal paraelectric at room temperature. This further supports the fact that these are cubic at room temperature. No further investigation was done. Existence of ferroelectric loop was the only concern of study.

A lower remnant polarization and smaller coercive field has been reported to be due to increase in domain pinning by residual vacancies [34,37,50]. Under the applied electric field some oxygen vacancies may hop to lower free energy sites such as domain walls and interfaces with electrodes. This generally weakens the defect mobility and contributing to domain pinning and decrease the remnant polarization and coercive field values. Appearance of secondary phase at the grain boundaries in the ceramics with higher Yb content may also have a contribution in domain pinning. It has also been reported that the random electric field around the defects lowers the barrier energy required for domain nucleation, decreasing the coercive field [51].

Effect of grain size also cannot be neglected. It has been reported that larger grains have larger remnant polarization as domain walls among larger grains are easier to switch under external electric field [52]. In the prepared ceramics as Yb content increases grain size decreases, energy barrier and number of grain boundary increases. Now grain boundary is a low permittivity region having poor ferroelectricity. Hence remnant polarization decreases too along with increase in Yb content.

The photoluminescence (PL) emission spectra of undoped and doped BT were examined at room temperature irradiated with ultraviolet radiation at 250 nm with a 290 nm filter. The PL curves shown in Fig. 11 can be classified into five PL components, violet maximum below 418 nm, blue maximum below 448 nm, green maximum below 493 nm, yellow maximum below 577 nm, and red maximum below 657 nm, in allusion to the regions where the component's maxima appear [53]. Undoped and doped ceramics show peak at 400 nm, which broadens with subsequent increase in Yb content. Some small peaks at 451 nm, 470 nm, 484 nm, 494 nm are also observed. Clearly these materials belong to the zone of violet, blue and green maximum. Neither shifting of these peaks nor broadening is observed on doping and even on increasing the content of Yb. Undoped BT has been reported to show photoluminescence peak in the UV region at 396 nm, which is quite close to our observations [54].

Luminescence of pure BT has generally been described to be due to self-trapped excitons. The electronic band structure of BT has low-lying narrow conduction bands from Ti-3d states and valence bands from O-2p states [44,55]. The energy corresponding to 250 nm line makes a direct transition of electrons from valence band to conduction band followed by some decay mechanism resulting in the luminescence.

To exhibit room temperature PL, a system must have at least two types of differently charged clusters creating local polarization within the structure and/or some localized states existing in the band gap that directly affect the degree of order–disorder. The junction of these two conditions allows an easy trapping of electrons and holes during excitations causing PL emission. In ABO_3 perovskites structure, displacement of A and B atoms together or separately produces a disordered system or structural asymmetry. This induces destabilization of their atomic orbitals as well as of the oxygen orbital (Jahn–Teller effect) [56] leading to intermediate states in the forbidden band gap and hence reduction of the gap values. This favors the appearance of small polarons in the gap region. These polarons interact with holes trapped in the crystal (defects or impurities) and form self-trapped excitons [57,58]. When Yb is doped in BT, a modification in the position of B-site ion and also A-site ion occurs simultaneously leading to displacements in Ti–O/Yb–O, Ba–O bonds

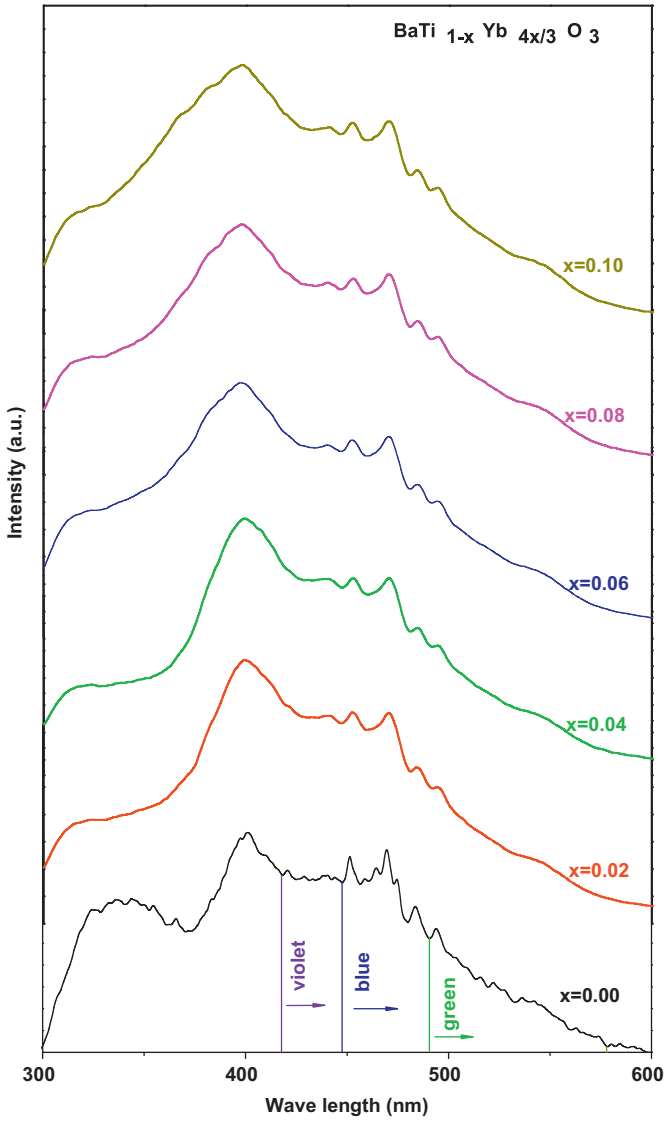

Fig. 11. Room temperature photoluminescence emission spectra of $BaTi_{1-x}Yb_{4x/3}O_3$.

that ensures Jahn–Teller effect. In the first state i.e. the excitation process in the Yb doped ceramics electrons from the O-2p valence band absorb energy from the incident wavelength (λ=250 nm) and are promoted to Ti-3d/Yb-4f conduction band. Electrons come back to the lower energy state via radiative decay leading to emission. The broadening in the emission peak at 400 nm upon subsequent Yb doping indicates that the charge transfer process via defects as well as the trapping of electrons is occurring [59]. Again, luminescence properties in Yb based ceramics have been attributed to ($^2F_{5/2} \rightarrow {}^2F_{7/2}$) transitions in the 4f electronic shell of Yb^{3+} ions [60]. Thus multiple phenomena including intra 4f transition in the Yb^{3+} ions are responsible for the PL properties in the Yb doped compositions.

If the degree of local order in a system is such that structurally inequitable sites can be distinguished by different types of electronic transitions then these different types of electronic transitions are linked to a specific structural arrangement. Red component represents the less energetic electronic transitions and are thus linked to states that are deeply inserted in the band gap. Conversely, the blue component, more energetic, is linked to shallow defects in the band gap. Since the prepared materials are found to belong to the zone of violet, blue and green maximum, it is clear that formation of shallow defects in the band gap of BT takes place due to Yb doping.

The DR spectra of all the prepared ceramics after Kubelka–Munk treatment are shown in Fig. 12. The detailed theory behind has been given in earlier works [34,61]. The E_{gap} values were evaluated by extrapolating the linear portion of the curve or tail and are found to decrease with subsequent increase in Yb content.

The obtained E_{gap} values for the doped ceramics can be associated with the distortions in the [TiO_6] clusters and other structural disorder, as already explained, introduced into the lattice due to Yb incorporation. Distortions introduce shallow defects in the band gap of BT decreasing the value. With increase in Yb content distortion in the TiO_6 octahedron increases along with and formation of larger number of shallow defects takes place. Hence band gap decreases further [57]. The band gap of pure BT in normal conditions lies between 3.2 and 3.5 eV. But here a low value is obtained. This may be due to oxygen vacancies, lattice defects and/or local bond distortion which yield localized electronic levels in the band gap of the material [62]. Deep holes (between the valence band and conduction band with small E_{gap} values) are responsible for the green, yellow, orange and red PL emission at room temperature, while the shallow holes (between the valence band and conduction band with high E_{gap} values) promote the violet and blue emissions [57]. Clearly, formation of shallow defects is the reason behind optical characteristics.

4. Conclusions

$Ba(Ti_{1-x}Yb_{4x/3})TiO_3$ (x=0.02, 0.04, 0.06, 0.08 and 0.10) were prepared by the solid state reaction route. Rietveld Refinement confirm a compositionally induced phase transition from tetragonal to cubic symmetry in x=0.06. The same is supported through FTIR, Raman spectroscopy and temperature dependent dielectric study. FTIR study reveals distortion in the TiO_6 octahedra due to Yb substitution. Decrease in intensity, followed by a disappearance of the tetragonal Raman modes and appearance of extra peaks at higher frequency sides of existing peaks occur with subsequent increase in Yb^{3+} ion content. Presence of Yb is found to strongly modify the microstructure. A drastic decrease in grain size is observed with subsequent increase in Yb concentration, especially from $x \geq 0.06$. Dielectric study shows normal ferroelectric character for $x \leq 0.04$ with drastic decrease in Curie temperature while x=0.06 shows a non-relaxor DPT. An increase in the degree of relaxation strength is observed at x=0.08 and 0.10 showing good $V \sim F$ fit. Formation of micro-domains with local polarizations along with appearance of secondary phase may induce such behavior at 6% Yb concentration. P–E hysteresis loops show a successive decrease in remnant polarization

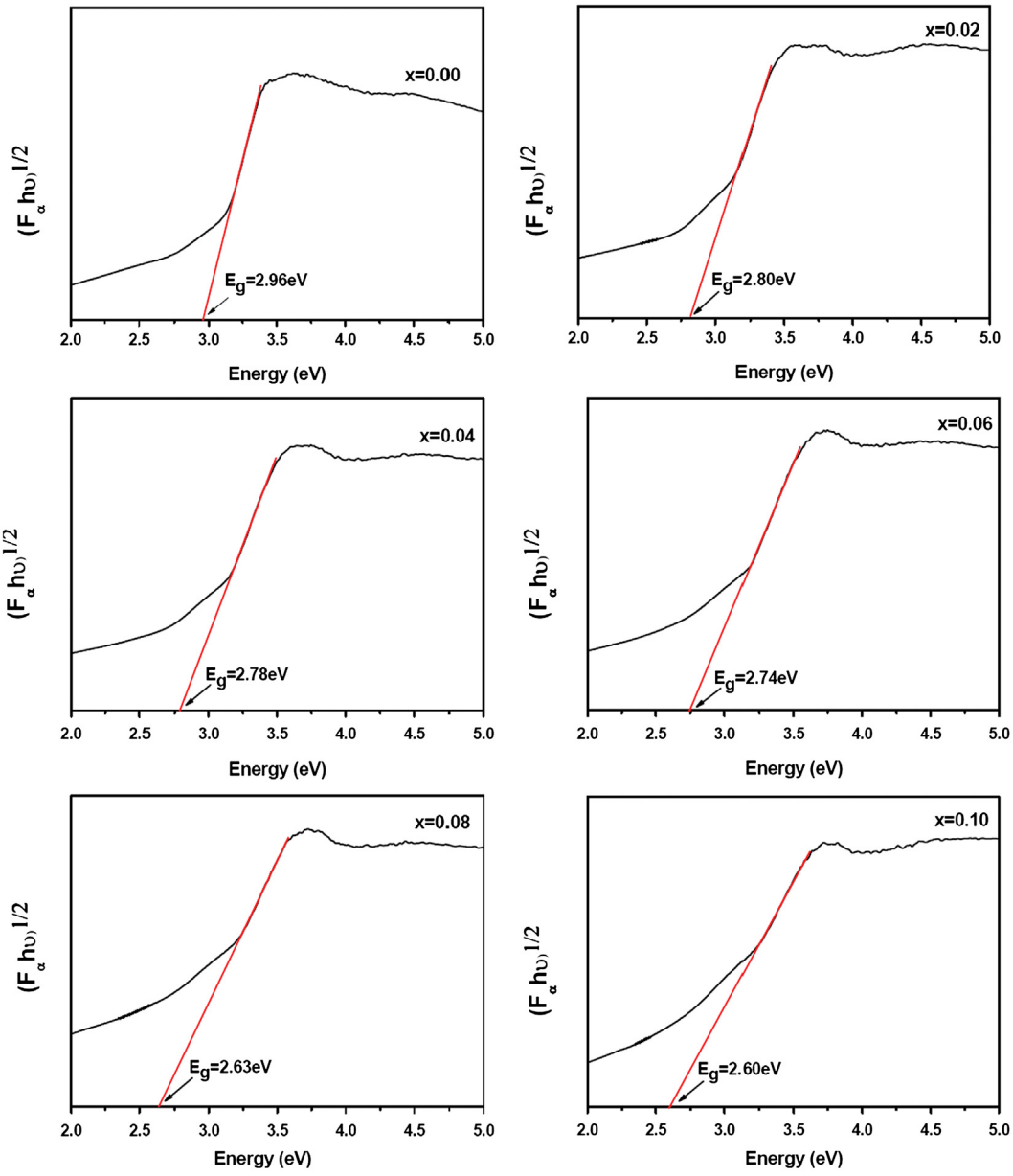

Fig. 12. Room temperature UV–vis absorbance spectrum of $BaTi_{1-x}Yb_{4x/3}O_3$.

values with subsequent Yb substitution due to domain pinning. The hysteresis behavior is in accordance with the microstructural behavior showing a good grain size effect on the remnant polarisaton and coercive field values. A paraelectric behavior is traced in $x \geq 0.06$. Photoluminescence emission spectra recorded at room temperature show structural distortion that generates asymmetry and self-trapped excitons. UV–visual study reveals a successive decrease in band gap values which may be due to formation of shallow defects in the forbidden gap.

References

[1] H. Kishi, Y. Mizuno, H. Chazono, Base-metal electrode-multilayer ceramic capacitors: past, present and future perspective, Japanese Journal of Applied Physics 42 (2003) 1–15.

[2] A.J. Moulson, J.M. Herbert, Electroceramics: Materials, Properties, and Applications, Chapman-Hall, London, 1990.

[3] S.B. Narang, D. Kaur, Dielectric investigations of lanthanides (Ln = Sm, Nd and Gd) substituted barium titanate microwave ceramics, Integrated Ferroelectrics 105 (2009) 87–98.

[4] D.Y. Lu, T. Koda, H. Suzuki, M. Toda, Dielectric temperature characteristics of high-k (Ba,La) (Ti,Ce) O_3 ceramics, Journal of the Ceramic Society of Japan 113 (2005) 721–727.

[5] H. Ohsato, H. Kato, M. Mizuta, S. Nishigaki, T. Okuda, Microwave dielectric properties of $Ba_{6-3x}(Sm_{1-y}R_y)_{8+2x}Ti_{18}O_{54}$ (R = Nd and La) solid-solutions with zero temperature co-efficient of the resonant frequency, Japanese Journal of Applied Physics 34 (1995) 5413–5417.

[6] D. Kolar, S. Gaberscek, B. Volavsek, H.S. Parker, R.S. Roth, Synthesis and crystal chemistry of $BaNd_2Ti_3O_{10}$, $BaNd_2Ti_5O_{14}$ and $Nd_4Ti_9O_{24}$, Journal of Solid State Chemistry 38 (1981) 158–164.

[7] M. Valant, D. Sovorov, D. Kolar, X-ray investigations and determination of the dielectric properties of the compound $Ba_{4.5}Gd_9Ti_{18}O_{54}$, Japanese Journal of Applied Physics 35 (1996) 144–150.

[8] H. Ohsato, T. Ohhashi, T. Okuda, K. Sumiya, S. Suzuki, Lattice parameters of bronze-type $3BaO–2R_2O_3–9TiO_2$(R=Sm and Nd) solid-solution for microwave dielectric ceramics, Advances in X-Ray Analysis 37 (1994) 79–85.
[9] S. Garcia, R. Font, J. Portelles, R.J. Quinones, J. Heiras, J.M. Siqueiros, Effect of Nb doping on (Sr,Ba)TiO_3 (BST) ceramic samples, Journal of Electroceramics 6 (2001) 101–108.
[10] M. Aparna, T. Bhimasankaram, S.V. Suryanarayana, G. Prasad, G.S. Kumar, Effect of lanthanum doping on electrical and electromechanical properties of $BaTiO_3$, Bulletin of Materials Science 24 (2001) 497–504.
[11] T. Murakami, T. Miyashita, M. Nakahara, E. Sekine, Effect of rare-earth ions on electrical conductivity of $BaTiO_3$ ceramics, Journal of the American Ceramic Society 56 (1973) 294–297.
[12] S.M. Rhim, S. Hong, H. Bak, O. Kim, Effects of B_2O_3 addition on the dielectric and ferroelectric properties of $Ba_{0.7}Sr_{0.3}TiO_3$ ceramics, Journal of the American Ceramic Society 83 (2000) 1145–1148.
[13] Y. Tsur, T.D. Dunbar, C.A. Randall, Crystal and defect chemistry of rare earth cations in $BaTiO_3$, Journal of Electroceramics 7 (2001) 25–34.
[14] T.D. Dunbar, W.L. Warren, B.A. Tuttle, C.A. Randall, Y. Tsur, Electron paramagnetic resonance investigations of lanthanide-doped barium titanate: dopant site occupancy, Journal of Physical Chemistry B 108 (2004) 908–917.
[15] W. Li, J. Qi, Y. Wang, L. Li, Z. Gui, Doping behaviors of Nb_2O_5 and Co_2O_3 in temperature stable $BaTiO_3$-based ceramics, Materials Letters 57 (2002) 1–5.
[16] C. Ma, X.H. Wang, R.Z. Chen, L.T. Li, Z.L. Gui, The effect of different doping methods of sintering aids on the barium titanate based X7R ceramics, Key Engineering Materials 83 (2007) 336–338.
[17] A. Honda, S. Higai, Y. Motoyoshi, N. Wada, H. Takagi, Theoretical study on interactions between oxygen vacancy and doped rare-earth elements in barium titanate, Japanese Journal of Applied Physics 50 (2011) 09NE01.
[18] F. Jona, G. Shirane, Ferroeletric Crystals, Pergamon, Dover Publication, New York, 1962 (reprinted in 1993).
[19] Z. Jing, C. Ang, Z. Yu, P.M. Vilarinho, J.L. Baptista, Incorporation of yttrium in barium titanate ceramics, Journal of the American Ceramic Society 82 (1999) 1345–1348.
[20] D.F.K. Hennings, B. Schreinemacher, H. Schreinemacher, High-permittivity dielectric ceramics with high endurance, Journal of the European Ceramic Society 13 (1994) 81–88.
[21] Y. Park, Y. Kim, The dielectric temperature characteristics of additives modified barium titanate having core–shell structured ceramics, Journal of Materials Research 10 (1995) 2770–2776.
[22] D. Makovec, Z. Samardaija, D. Kolar, Solid solubility of cerium in $BaTiO_3$, Journal of Solid State Chemistry 123 (1996) 30–38.
[23] S. Wada, S. Suzuki, T. Noma, T. Suzuki, M. Osada, M. Kakihana, S.E. Park, L.E. Cross, T.R. Shrout, Enhanced piezoelectric property of barium titanate single crystals with engineered domain configurations, Japanese Journal of Applied Physics 38 (1999) 5505–5511.
[24] Y. Zhi, R. Guo, A.S. Bhalla, Orientation dependene of the ferroelectric and piezoelectric behavior of $Ba(Ti_{1-x}Zr_xO_3)$ single crystals, Applied Physics Letters 77 (2000) 1535–1537.
[25] V.V. Mitic, Z.S. Nikolic, V.B. Pavlovic, V. Paunovic, M. Miljkovic, B. Jordovic, L. Zivkovic, Influence of rare earth dopants on barium titanate ceramics microstructure and corresponding electrical properties, Journal of the American Ceramic Society 93 (2010) 132–137.
[26] G. Yao, X. Wang, Y. Yang, L. Li, Effects of Bi_2O_3 and Yb_2O_3 on the Curie temperature in $BaTiO_3$-based ceramics, Journal of the American Ceramic Society 93 (2010) 1697–1701.
[27] Y. Li, Y. Hao, X. Wang, X. Yao, Studies of dielectric properties of rare earth (Y, Gd, Yb) doped barium titanate sintered in pure nitrogen, Ferroelectrics 407 (2010) 134–139.
[28] A.G. Murillo, F.J.C. Romo, M.G. Hernandez, J.R. Salgado, M.A. D. Crespo, S.A.P. Sanchez, H. Terrones, Structural and morphological characteristics of polycrystalline $BaTiO_3$:Er^{3+}, Yb^{3+} ceramics synthesized by the sol–gel route: influence of chelating agents, Journal of Sol-Gel Science and Technology 53 (2010) 121–133.
[29] S. Wang, S. Zhang, X. Zhou, B. Li, Z. Chen, Effect of sintering atmospheres on the microstructure and dielectric properties of Yb/Mg co-doped $BaTiO_3$ ceramics, Materials Letters 59 (2005) 2457–2460.
[30] C.H. Perry, B.N. Khanna, G. Rupprecht, Infrared studies of perovskite titanates, Physical Review 135A (1964) 408–412.
[31] R.A. Nyquist, R.O. Kagel, Infrared Spectra of Inorganic Compounds, Academic Press, New York, 1971.
[32] C. Ostos, L. Mestres, M.L. Martınez-Sarrion, J.E. Garcıa, A. Albareda, R. Perez, Synthesis and characterization of A-site deficient rare-earth doped $BaZr_xTi_{1-x}O_3$ perovskite-type compounds, Solid State Sciences 11 (2009) 1016–1022.
[33] X. Jin, D. Sun, M. Zhang, Y. Zhu, J. Qian, Investigation on FTIR spectra of barium calcium titanate ceramics, Journal of Electroceramics 22 (2009) 285–290.
[34] M. Ganguly, S.K. Rout, H.Y. Park, C.W. Ahn, I.W. Kim, Structural, dielectric and optical characterization of cerium doped barium titanate, Physics Express 3 (2013) 1–12.
[35] Y. Liu, Y. Feng, X. Wu, X. Han, Microwave absorption properties of la doped barium titanate in X-band, Journal of Alloys and Compounds 472 (2009) 441–445.
[36] P.S. Dobal, A. Dixit, R.S. Katiyar, Effect of lanthanum substitution on the raman spectra of barium titanate thin films, Journal of Raman Spectroscopy 38 (2007) 142–146.
[37] Y.I. Yuzyuk, V.A. Alyoshin, I.N. Zakharchenko, E.V Sviridov, A. Almeida, M.R. Chaves, Polarization-dependent raman spectra of heteroepitaxial (Ba,Sr)TiO_3/MgO thin films, Physical Review B 65 (2002) 134107.
[38] D. Rout, Structural, electrical and raman spectroscopic studies of lead ytterbium tantalate based ceramics, IIT Madras, Chennai, 2006 (Ph.D. thesis).
[39] M. Correa, A. Kumar, S. Priya, R.S. Katiyar, J.F. Scott, Phonon anomalies and phonon-spin coupling in oriental $PbFe_{0.5}Nb_{0.5}O_3$ thin films, Physical Review B 83 (2011) 014302.
[40] U.D. Venkateswaran, V.M. Naik, R. Naik, High-pressure Raman studies of polycrystalline $BaTiO_3$, Physical Review B 58 (1998) 14256–14260.
[41] S.Y. Wang, B.L. Cheng, C. Wang, S.Y. Dai, K.J. Jin, Y.L. Zhou, H.B. Lu, Z.H. Chen, G.Z. Yang, Raman spectroscopy studies of ce-doping effects on $Ba_{0.5}Sr_{0.5}TiO_3$ thin films, Journal of Applied Physics 99 (2006) 013504.
[42] S.K. Jo, J.S. Park, Y.H Han, Effects of multi-doping of rare-earth oxides on the microstructure and dielectric properties of $BaTiO_3$, Journal of Alloys and Compounds 501 (2010) 259–264.
[43] S.M. Bobade, D.D. Gulwade, A.R. Kulkarni, P. Gopalan, Dielectric properties of A- and B-site-doped $BaTiO_3$: La- and Al-doped solid solutions, Journal of Applied Physics 97 (2005) 074105.
[44] J. Yu, J. Sun, J. Chu, D. Tang, Light emission properties in nanocrystalline $BaTiO_3$, Applied Physics Letters 77 (2000) 2807–2809.
[45] K. Alioune, A. Guehria-Laidoudi, A. Simon, J. Ravez, Study of new relaxor materials in $BaTiO_3$–$BaZrO_3$–$La_{2/3}TiO_3$ system, Solid State Sciences 7 (2005) 1324–1332.
[46] F.D. Morrison, D.C. Sinclair, A.R. West, Electrical and structural properties of characteristics of lanthanum-doped barium titanate ceramics, Journal of Applied Physics 86 (1999) 6355–6366.
[47] S. Kumar, K.B.R. Varma, Influence of lanthanum doping on the dielectric, ferroelectric and relaxor behavior of barium bismuth titanate ceramics, Journal of Physics D: Applied Physics 42 (2009) 075405.
[48] D. Viehland, S. Jang, L.E. Cross, The dielectric relaxation of lead magnesium niobate relaxor ferroelectrics, Philosophical Magazine Part B 64 (1991) 335–344.
[49] J. Ravez, A. Simon, Some solid state chemistry aspects of lead-free relaxor ferroelectrics, Journal of Solid State Chemistry 162 (2001) 260–265.
[50] M. Ganguly, S. Parida, E. Sinha, S.K. Rout, A.K. Himansu, A. Hussain, I.W. Kim, Structural, dielectric and electrical properties of $BaFe_{0.5}Nb_{0.5}O_3$ ceramic prepared by solid-state reaction technique, Materials Chemistry and Physics 131 (2011) 535–539.

[51] D. Viehland, Y.H. Chen, Random-field model for ferroelectric domain dynamics and polarization reversal, Journal of Applied Physics 88 (2000) 6696–6707.
[52] W. Cai, C. Fu, J. Gao, H. Chen, Effects of grain size on domain structure and ferroelectric properties of BZT ceramics, Journal of Alloys and Compounds 480 (2009) 870–873.
[53] V.M. Longo, L.S. Cavalcante, A.T. de Figueiredo, L.P.S. Santos, E. Longo, J.A. Varela, J.R. Sambrano, C.A. Paskocimas, F.S. De Vicente, A.C. Hernandes, Highly intense violet–blue light emission at room temperature in structurally disordered $SrZrO_3$ powders, Applied Physics Letters 90 (2007) 091906.
[54] T. Sahoo, S.K. Tripathy, S. Nandy, B. Pandey, H.C. Verma, K.K. Chattopadhyay, S. Ananda, Microstructural and photo luminescence studies on hydrothermally synthesized Ce-doped barium titanate nanocrystals, Materials Science and Engineering: B 131 (2006) 277–280.
[55] E. Orhan, V.C. Albarici, M.T Escote, M.A.C. Machado, P.S. Pizani, E.R. Leite, J.R. Sambrano, J.A. Varela, E. Longo, A DFT rationalization of the room temperature photoluminescence of Li_2TiSiO_5, Chemical Physics Letters 398 (2004) 330–335.
[56] E. Orhan, F.M. Pontes, E.R. Leite, P.S. Pizani, J.A. Varela, E. Longo, Experimental and theoretical investigation of the room-temperature photoluminescence of amorphized $Pb(Zr,Ti)O_3$, ChemPhysChem 6 (2005) 1530–1536.
[57] M.L. Moreira, M.F.C. Gurgel, G.P. Mambrini, E.R. Leite, P.S. Pizani, J.A. Varela, E. Longo, Photoluminescence of barium titanate and barium zirconate in multilayer disordered thin films at room temperature, Journal of Physical Chemistry A 112 (2008) 8938–8942.
[58] R. Leonelli, J.L. Brebner, Time resolved spectroscopy of the visible emission band in strontium titanate, Physical Review B 33 (1986) 8649–8656.
[59] J.C. Sczancoski, L.S. Cavalcante, T. Badapanda, S.K. Rout, S. Panigrahi, V.R. Mastelaro, J.A. Varela, M.S. Li, E. Longo, Structure and optical properties of $[Ba_{1-x}Y_{2x/3}](Zr_{0.25}Ti_{0.75})O_3$ powders, Solid State Sciences 12 (2010) 1160–1167.
[60] A.G. Murillo, F.J.C. Romo, M.G. Hernandez, O.B. Garcia, A.M. Nava, S.P. Sanchez, A.F. Vela, Structural and optical characteristics of $BaTiO_3$: Yb^{3+} powders, Materials Transactions 50 (2009) 1850–1854.
[61] A.E. Morales, E.S. Mora, U. Pal, Use of diffuse reflectance spectroscopy for optical characterization of un-supported nanostructures, Revista Mexicana de F´isica 53 (2007) 18–22.
[62] V.M. Longo, A.T. Figueiredo, S.de Lázaro, M.F. Gurgel, M.G S. Costa, C.O. Paiva-Santos, J.A. Varela, E. Longo, V. Mastelaro, R.F.S. de Vicente, A.C. Hernandes, R.W.A. Franco, Structural conditions that leads to photoluminescence emission in $SrTiO_3$: an experimental and theoretical approach, Journal of Applied Physics 104 (2008) 023515.